On the growth and structure of Al2O3-Y3Al5O12-ZrO2:Y solidified eutectic

M. Cherif, Thierry Duffar, L. Carroz, P. Lhuissier, E. Bautista-Quisbert

Version of Record: https://www.sciencedirect.com/science/article/pii/S0955221920302053
Manuscript_b9c1cf08e45f80e7c11776d0718885ce

On the growth and structure of Al_2O_3-$Y_3Al_5O_{12}$-ZrO_2:Y solidified eutectic

M. Cherif [1, *], T. Duffar[2, +], L. Carroz[1, *], P. Lhuissier[2], E. Bautista-Quisbert[2]

[1] Safran Aircraft Engines, Rond-point René Ravaud, 77550 Moissy Cramayel, France

[2] Univ. Grenoble Alpes, CNRS, Grenoble INP, SIMAP, 38000 Grenoble, France

[+] Corresponding author: thierry.duffar@grenoble-inp.fr

* Presently at Industeel-CRMC, Le Creusot, France

Abstract

Structural features of Al_2O_3-YAG-ZrO_2:Y eutectic plates grown by the EFG process have been studied. X-ray tomography shows that all three phases are continuous along the whole sample, suggesting a fully coupled ternary eutectic growth. However the growth of alumina and YAG is well described by a classical binary coupled growth, in spite of the facetted structure of their growth interface. Colonies are observed at high growth rate and have been related to the chemical rejection of zirconium ions at the solid-liquid interface, possibly due to a slight off-stoechiometry of the raw material.

Keywords

Al_2O_3-YAG-ZrO_2 eutectic ceramic; microstructure; eutectic solidification; colonies.

1. Introduction

In 1996, Waku et al. [1] compared the mechanical properties of various materials for high temperature turbine blades: sintered and solidified binary eutectic alloys, Al_2O_3-$Gd_3Al_5O_{12}$, Al_2O_3-$Y_3Al_5O_{12}$ and Ni-based alloys. They found that solidified oxide eutectics

present a higher working temperature, thanks to their entangled microstructure, called Chinese script, and to the quality of the interphase surfaces. Thermal stability, mechanical properties, creep resistance and rupture stress remain constant until temperatures close to the melting point, 2000 K. By the way, control of the solidification process allows growing single crystal phases extending all along the ingot. Addition of ZrO_2:Y to the Al_2O_3-$Y_3Al_5O_{12}$ eutectic further increased the material toughness, so that this ternary eutectic remains one of the best candidates for high stress and high temperature uses. In this eutectic, $Y_3Al_5O_{12}$ (YAG) and alumina major phases have volume fractions, respectively, of 42 % and 40 % while zirconia occupies 18 % [2]. Our work is aiming to improve the understanding of the growth of the Al_2O_3-YAG-ZrO_2:Y eutectic with special attention to the Chinese Script structure.

A first point concerns the exact structure of the eutectic. It is generally accepted that eutectics grow in a coupled way, i.e. the phases are continuously growing thanks to inter-diffusion of the components. By the way, SEM observation of etched samples [3] and structural X-Ray tomographies [4] revealed that the three phases are continuous. In order to check the phase continuity in our samples and evaluate the effect of after-growth cooling on the entangled structure, further tomography experiments are performed and reported in the second section. Experimental studies have shown that the ternary eutectics follow a classical $\lambda^2 V = Cte$ relationship. However, the alumina and YAG phases grow from the melt in a facetted mode and understanding of the facetted/facetted eutectic growth, binary or ternary, is not well advanced. This will be addressed in the third section. Another aspect of the structure concerns the occurrence of colonies at high growth rate that are deleterious to the mechanical properties of the material; they will be studied in the fourth part. Finally, these observations will be discussed in the last section, in order to propose a general understanding of the growth of this eutectic material.

2. Experimental

The samples studied in this work have been produced by the Edge defined Film-fed Growth (EFG) technique in a Cyberstar puller at the RSA company premises. This growth process is commonly used for industrial production of sapphire plates and rods. Adaptation of the sapphire growth equipment, crucible, die and procedure to the pulling of Al_2O_3-YAG-ZrO_2:Y eutectic plates is discussed in [5] and explained in more details in [6]. Plates, dimensions 220 mm-36 mm-4 mm, were then routinely produced with growth rates ranging from 1 to 10 µm.s^{-1}. As measured with a thermocouple travelling with the seed [5] and in agreement with numerical simulation of heat transfer in the furnace [7-8], temperature gradients at the solid-liquid interface were of the order 100 K.cm^{-1} in the solid and 35 K.cm^{-1} in the liquid.

The raw material was elaborated by the "Centre de Transfert de Technologies Céramiques" platform, by careful mixing, isostatic hot-pressing and sintering of Al_2O_3, Y_2O_3 and ZrO_2 powders in eutectic proportions. However, disparities of eutectic composition and temperature in the literature (Table 1) introduce a difficulty in the elaboration process. Two batch feedstock were used. Their chemical composition was measured by ICP for the metal and, for the oxygen, by infrared measurement of CO produced by reaction with a graphite crucible. While they show differences in composition and solidification temperature (obtained by TDA), they are close to the published values and no significant difference in terms of obtained microstructures was noticeable after solidification. The resulting EFG-grown material do not show significant chemical composition differences, while a lower solidification temperature is measured.

Solidification Temperature (K)	Chemical composition (Molar fraction) Al_2O_3	ZrO_2	Y_2O_3	Reference
1988	0,651	0,179	0,170	Calphad database TCOX5
1996	0,664	0,177	0,158	[9]
1988	0,650	0,190	0,160	[10]
1988	0,658	0,186	0,156	[11]
1991	0,646	0,191	0,163	This study, batch #1 feedstock
1990	0,652	0,187	0,161	This study, batch #2 feedstock
1965	0,650	0,189	0,161	This study, EFG plate, middle part
1973	0,640	0,194	0,166	This study, EFG plate, end
1984	0,646	0,194	0,160	This study, sampling of remaining liquid

Table 1: Eutectic compositions and temperature of the Al_2O_3-ZrO_2-Y_2O_3 system.

This work was part of a more general research project in which Al_2O_3-YAG-ZrO_2:Y eutectic samples were also grown from the melt by Bridgman [12] and Micro-pulling-down techniques [13]. The same raw batch materials were used. Samples obtained by the other techniques were characterized, similarly to the EFG samples, in terms of eutectic structure, eutectic spacing relationship and colony occurrence. Variance analysis of the Jackson-Hunt constant data showed that the growth process does not affect significantly (at the 0.01 confidence level) the eutectic structure, the eutectic spacing relationship and the colony occurrence, taking into account the different temperature gradients, also estimated by numerical simulation [7]. So that the EFG samples can be considered as fully representative of the solidification behavior in the growth rate range studied thanks to the three techniques: 0.25 to 15 µm.s^{-1}.

Depending on the characterization technique, described in the relevant sections, samples were cut with a diamond saw, roughed on a polymer-diamond disk then polished with diamond suspensions from 9 µm to 1 µm.

3. Tomography of the samples

Longitudinal and transverse sections (Figure 1) show that the alumina and YAG phases are elongated along the growth direction and show a classical Chinese Script structure. However, it is not possible to check the connectivity of the various phases on such images.

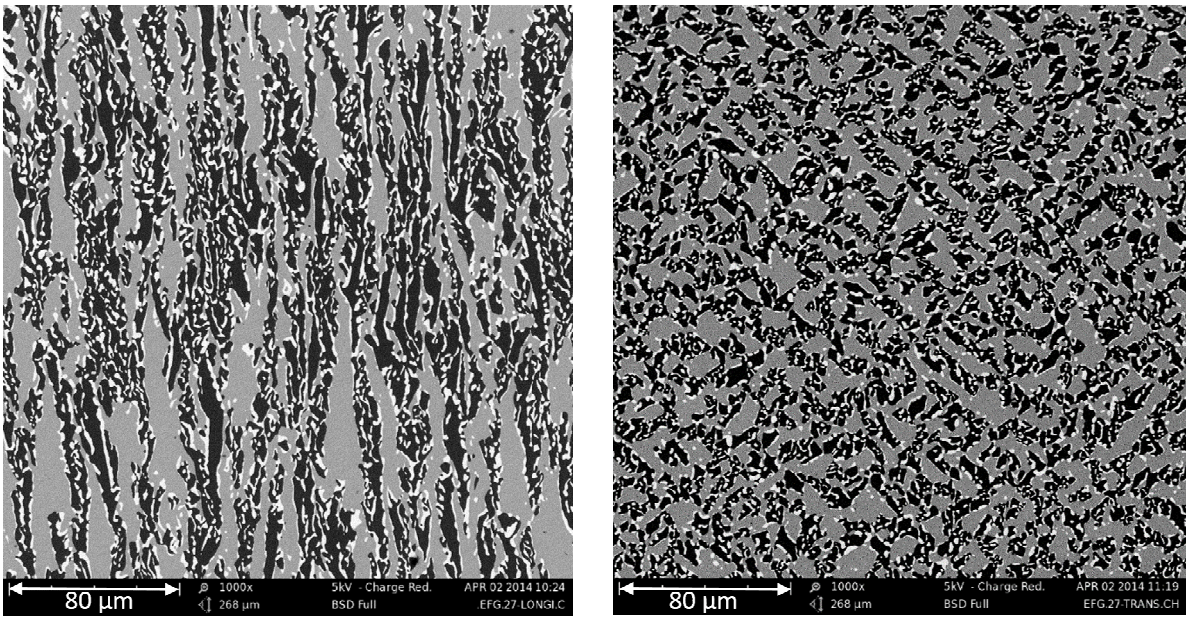

Figure 1: Longitudinal and transversal structure of a ternary eutectic sample grown by the EFG process (V= 2.5 10^{-6} $m.s^{-1}$) observed by SEM. Alumina is black, YAG grey and zirconia white.

An X-ray microtomograph Easytom XL Nano was used in order to investigate the eutectic structure. As the characteristic voxel size is of the order 300 nm, rather large structures should be analyzed, i.e. grown at low velocity. We used samples grown at 1.6 $x10^{-6}$ $m.s^{-1}$. The analyzed volume was 248x591x1892 voxels and images were produced with 255 grey level. They were analyzed with the Analyse3D plugin in the ImageJ software [14]. Figure 2 shows the three reconstructed tridimensional phases. Al_2O_3 and YAG are entangled lamellas oriented along the growth direction, as already observed by Murayama [15]. Several plates solidified by the EFG process were analyzed by X-ray diffraction, on various transversal cuts. They have shown that the longitudinal growth directions of the YAG and Al_2O_3 phases remain comparable from one plate to the other: respectively <100> and $<10\bar{1}0>$. The alloy is therefore constituted of two entangled single crystals. Some diffraction

results, however, have shown that several plates contain grain boundaries, without any obvious link to particular growth conditions.

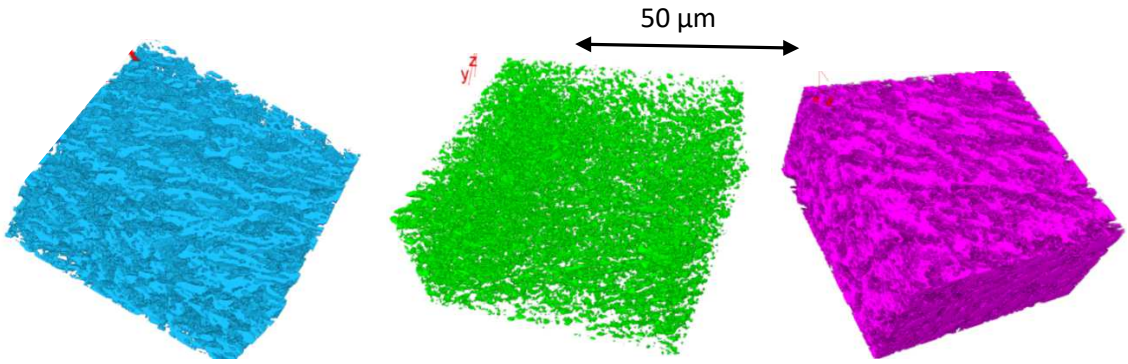

Figure 2: 3D morphologies of the phases reconstructed from X-ray microtomograph: Al_2O_3 (left), ZrO_2:Y (middle) and YAG (right). The EFG plate was pulled at 1.6 10^{-6} $m.s^{-1}$.

The discontinuity of the ZrO_2:Y is consistent with results reported from analysis of 2D images of ternary or binary (Al_2O_3-YAG) eutectics [16, 17], but not with the tomographic results presented in [3, 4]. Also, Merino [18], argued that the Y doped-zirconia phase should be continuous. She measured the electrical conductivity of the eutectic as 18% of the conductivity of Y-doped zirconia, a result consistent with the 16% fraction of zirconia in the eutectic.

In order to get a better resolution, experiments were performed on the beamline ID16B at the European Synchrotron Radiation Facility (ESRF), in Grenoble, France. Samples were obtained by cutting very small pieces, then grinding them. Finally, tiny samples with a needle-shape were carefully selected with the help of an optical microscope. Note that, due to this sampling procedure, samples are not aligned along the growth direction. Two samples were prepared, grown at 1.6 10^{-6} $m.s^{-1}$. The first one was extracted from the central part of an EFG plate which was grown and cooled down according to the regular pulling process.

However, the slow pulling rate and temperature gradient keep the solid, after growth, at high temperatures for long times. For example, 2 hours after solidification, the solid has

only been cooled by 110 K. This might impact the microstructure. Then, the second sample was taken from the bottom of a plate that has been suddenly separated from the die at the maximum shaft translation rate, in order to get a very fast cooling of the microstructure immediately after solidification.

The energy of the beam in the experiment was set to 17.6keV. About 1500 radiographies were obtained during the rotation of the samples from 0 to 180 ° in 15 minutes in average [19]. The size of a voxel is 34.876x34.876x34.876 nm^3, i.e. around 10^3 smaller than with the previously used Easytom equipment. From this data set, a stack of 2D images is produced and treated by ImageJ in order to get quantitative analyses.

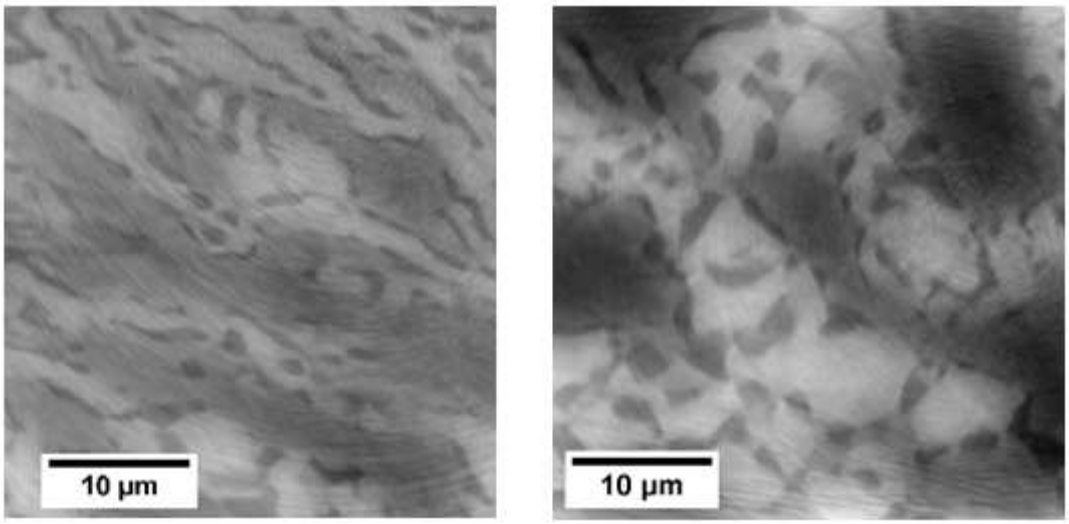

Figure 3: First layer of the transversal section showing the zirconia phase obtained by nano-tomography: rapidly cooled sample (left) and regular sample (right). Solidification rate was1.6 10^{-6} $m.s^{-1}$. Alumina appears in white, YAG in grey and zirconia is the darker phase.

In terms of microstructure, as figure 3 depicts, the zirconia distribution is affected by the plate cooling during growth. In the regularly solidified sample, the phase is bigger because aging and Oswald ripening had time to occur. On the other hand, in the rapidly cooled sample, the zirconia phase is smaller and more dispersed. The overall eutectic spacing is not significantly affected by the cooling regime.

Figure 4 shows how the phases change in the microstructure of the regularly pulled plate along the direction of solidification. From 250 pictures, spanning about 10 µm, only 15 equidistant pictures are shown. The small red ovals track $Zr0_2$ phase which appears to be continuous all along the examined 10 µm. This can be much easily seen on the videos produced by the animation tool in ImageJ, which use all the 250 layers [20]. Both regular and rapidly cooled samples show ZrO_2 continuity.

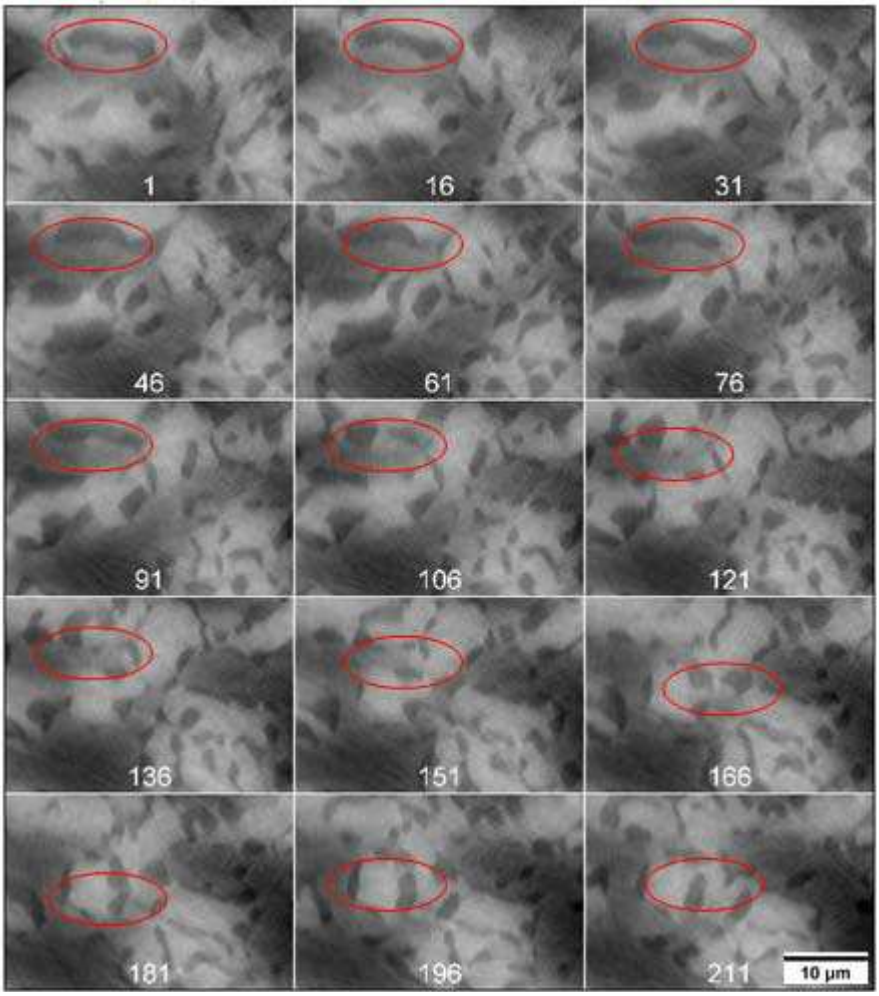

Figure 4: Selection of tomography images in the direction of growth of the EFG sample. Red ovals help following the ZrO_2 phase, which appears in dark gray color. The distance between two pictures is 510 nm. Solidification rate was1.6 10^{-6} $m.s^{-1}$and cooling was regular.

4. Eutectic spacing

It is well known that the Al_2O_3-YAG-ZrO_2:Y eutectic follows the classical relationship:

$$\langle\lambda\rangle^2 V = Cte, \quad (1)$$

where $\langle\lambda\rangle$ is the mean value of the eutectic spacing and V the solidification rate. The *Cte* value ranges from 2.8 10^{-17} $m^3.s^{-2}$ for Su et al. (up to 1. 10^{-4} $m.s^{-1}$) to 6.4 10^{-17} $m^3.s^{-2}$ for Lee et al. (up to 2.5 10^{-4} $m.s^{-1}$) [21, 22].

The discrepancy could be due to different methods used to measure the eutectic spacing. The irregularity of the Chinese script structure makes the determination of this spacing difficult, as the periodicity definition is ambiguous. By the way, the use of Fourier analysis on SEM images of our samples did not provide a clear value for the pattern periodicity. We used instead the intercepts method [23] for measuring the eutectic spacing, implemented in the ImageJ software. Strictly speaking, eutectic spacing is valid only for the YAG-alumina couple, as the zirconia phase appears discontinuous on the 2D images. We also tried to use the method from Mizutani et al. [11, 24], but the results were inconsistent, probably because of the complex shape of the structure.

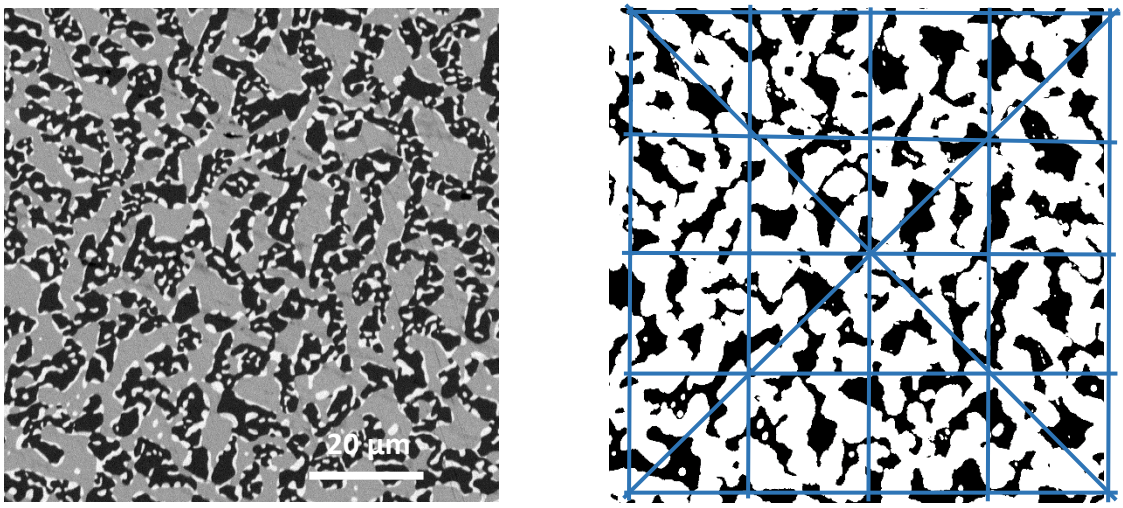

Figure 5: Left: Transversal cut of a sample grown at 3.3 10^{-6} $m.s^{-1}$ (YAG is the grey phase). Right: grid superimposed on the binarized image (black pixels: YAG, white pixels: Al_2O_3 and ZrO_2:Y).

In order to illustrate the intercept method, Figure 5 shows a transversal cut of a plate and the resulting binary image obtained after a set of treatments by the imageJ software, where only the YAG phase remains. Then a grid is superimposed on the image and the number and connectivity of intersected black or white pixels are measured on each line. This allows getting the YAG phase dimension, $\bar{t}_{YAG}$, and the distance between the YAG particules, after computing mean values. The same treatment is applied to the alumina phase, giving $\bar{t}_{Al_2O_3}$. Then the eutectic spacing is taken as:

$$\lambda = \bar{t}_{YAG} + \bar{t}_{Al_2O_3}. \quad (2)$$

Table 2 gives the measured spacing as function of the pulling rate. A statistical regression gives a value in agreement with [21, 22]:

$$(\lambda)^2 V = 8.10^{-17} \mathrm{m}^3.\mathrm{s}^{-1}. \quad (3)$$

Table 2: Growth rate effect on the mean size of the phases, on the eutectic spacing and on the colony diameter.

Growth rate (10^{-6} m.s^{-1})	$\bar{t}_{YAG}$ (µm)	$\bar{t}_{Al_2O_3}$ (µm)	λ (µm)	d_c (µm)
1.67	4.81 ± 1.	2.86 ± 0	7.67 ± 1	No colony
2.5	3.13 ± 0.	1.98 ± 0	5.11 ± 1	450 ± 20
3.33	2.87 ± 0.	1.96 ± 0	4.83 ± 0	330 ± 20
5.0	Not measured	Not measured	Not measured	220 ± 20
6.67	1.51 ± 0.	1.32 ± 0	2.83 ± 0	120 ± 20

5. Colonies

In the case of the Al_2O_3-YAG eutectic, there is a critical growth rate above which the structure changes from regularly distributed to colonies. These colonies have a eutectic structure in the center and larger spacing at the colony borders. Experimental results on different alumina-based eutectic alloys [25-31] have shown that the critical parameter is in fact the ratio $\left(\frac{G}{V}\right)_{crit.}$, suggesting that the mechanism of occurrence of colonies is linked to interface stability. However the nature of the destabilizing agent was not elucidated. Several hypotheses were proposed, including impurities [31, 32], off-eutectic composition [33] or evaporation of one component [34]. In the case of Al_2O_3-ZrO_2:Y eutectic, colonies are also observed and might be related to segregation of Y [21, 35-38], as Y-undoped Al_2O_3-ZrO_2 show colonies only for higher solidification rates [26].

In the case of the ternary eutectic, colonies were also observed, with a critical Temperature Gradient/Growth rate ratio [39-41]. Figure 6 shows the transverse cut of an EFG plate grown at $3.3.10^{-6}$ $m.s^{-1}$. Colonies are clearly visible.

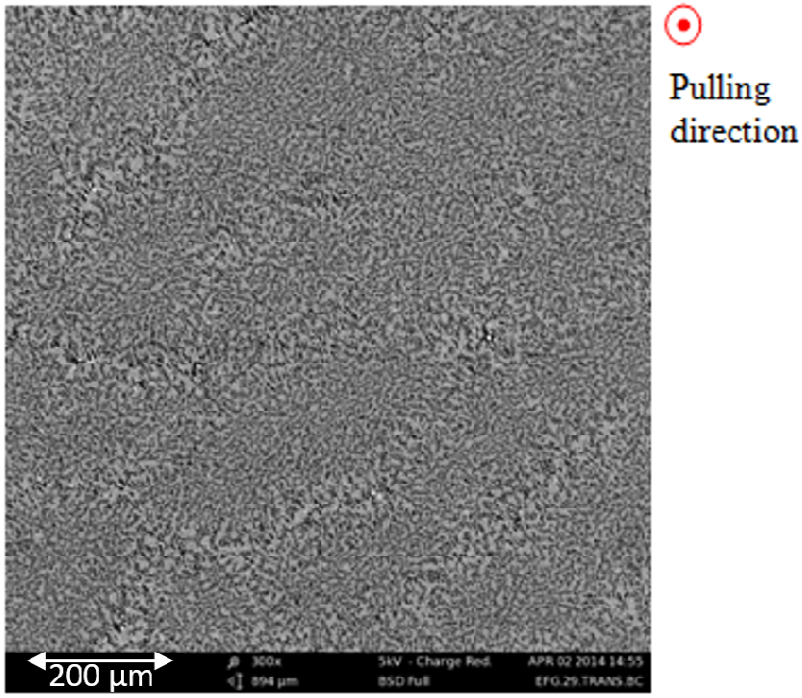

Figure 6: Transversal cut of a plate grown at $3.3.10^{-6}$ $m.s^{-1}$.

Following the work of Weart et Mack [42] on metallic eutectics, we computed the shape of the solidification front in case of colonies, under the hypothesis that the eutectic grows perpendicularly to this front. The change in eutectic spacing from the center to the periphery of a colony suggests that the growth rate decreases radially. Therefore, measuring the eutectic spacing variation along a colony diameter (Fig. 7-b)), and using Equation (3), allows plotting the growth rate as function of the diameter (Fig 7-c)). Considering the geometrical relationship:

$$V_{local} = V_{tip} \cos \theta, \qquad (4)$$

allows computation of the angle between the solidification interface and the pulling direction (fig. 7-d)). Finally the shape of the solidification front ahead a colony is plotted on Fig. 8. It appears that the interface morphology is not very much perturbed, likely because the destabilizing species is moderately segregated.

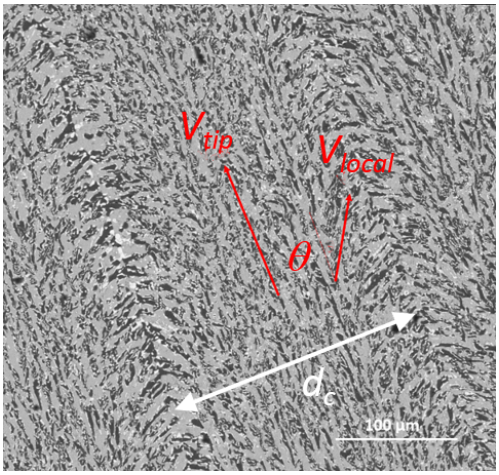

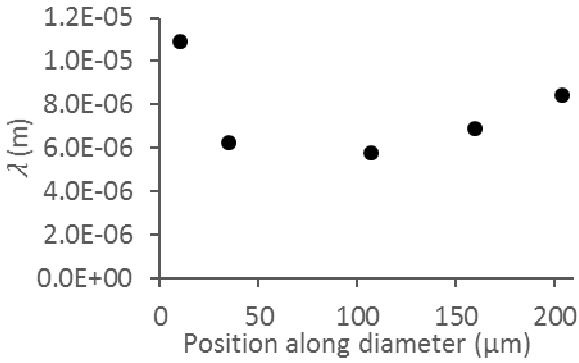

a) b)

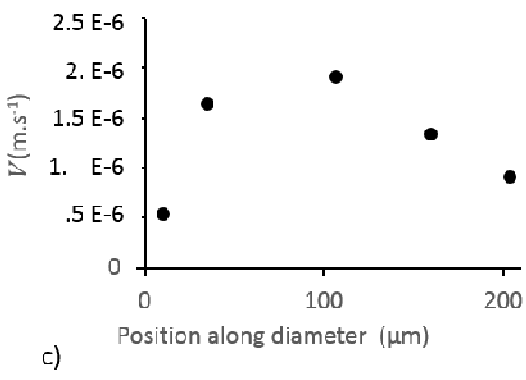

c)

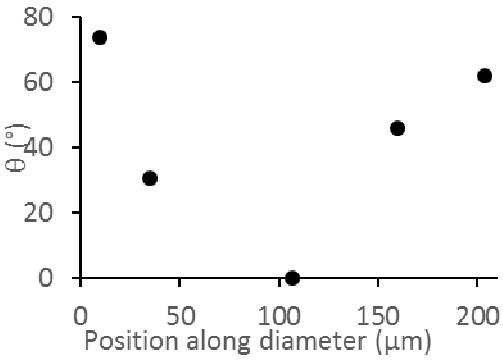

d)

Figure 7: Steps for reconstruction of the colony solidification interface. a) SEM image of a colony longitudinal cut (V=5. 10^{-6} $m.s^{-1}$). b) Eutectic spacing along the diameter d_c. c) Growth rate variation along d_c. d) Local angle of the solidification front toward growth direction.

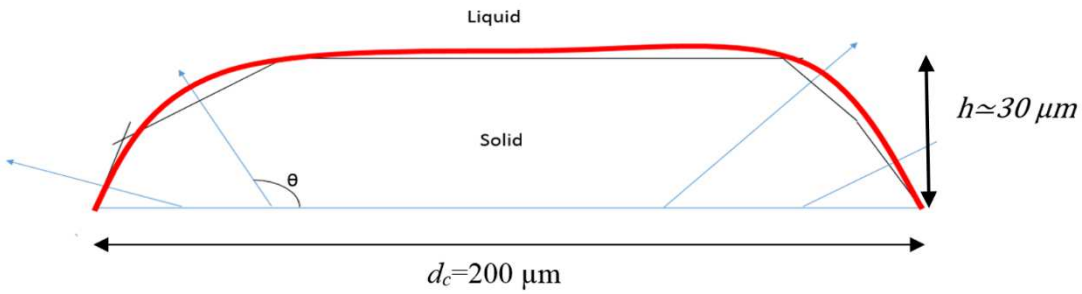

Figure 8: Shape of the solidification interface ahead a colony, in a plate pulled at $5x10^{-6}$m.s^{-1}.

The diameter of the colonies decreases when the growth rate increases (see table 2), following the relation:

$$d_c \sim V^{-1.2}, \qquad (5)$$

which gives a comparable but smallest exponent than the value, -1.6, calculated from the data published by Ester at higher growth rates, around 300 µm.s^{-1} [39].

The critical ratio Gradient/Growth rate was found to be $(1.4 \pm 0.3) \times 10^9$ K.m^{-2}.s, considering the computed temperature gradient of 35 K.cm^{-1}.

In order to elucidate the reason of the interface destabilization, we measured the electromotive force ahead the solid-liquid interface during growth and found that positive ions piled-up in the liquid. Further growth experiments of rods under an electric field, from our molten samples, showed that the zirconia phase was perturbed by the electric field. Switching-on the electric field promoted the precipitation of zirconia. These experiments and results are described and discussed in [43]. This agrees with the observation of ZrO_2 precipitates between the colonies (see white dots on figure 7-a), where the segregated species are rejected. Such observations suggess that the segregated species is Zr^{4+}, likely to be due to slight off-eutectic composition. Of course this is valid only for our raw material: destabilization in the case of other feedstock may be due to other factors.

6. Discussion

Figure 9-a) is a SEM picture of the structure obtained after a 10 time increase of the growth rate, in order to reveal the solid-liquid interface structure. It appears that the YAG (grey) phase is facetted and strongly protruding towards the melt. The alumina phase is depressed at the interface showing that it is not isothermal. Considering the rejection of Zr^{4+} (see section 5), our understanding of the solid-liquid interface morphology is shown on figure 9-b).

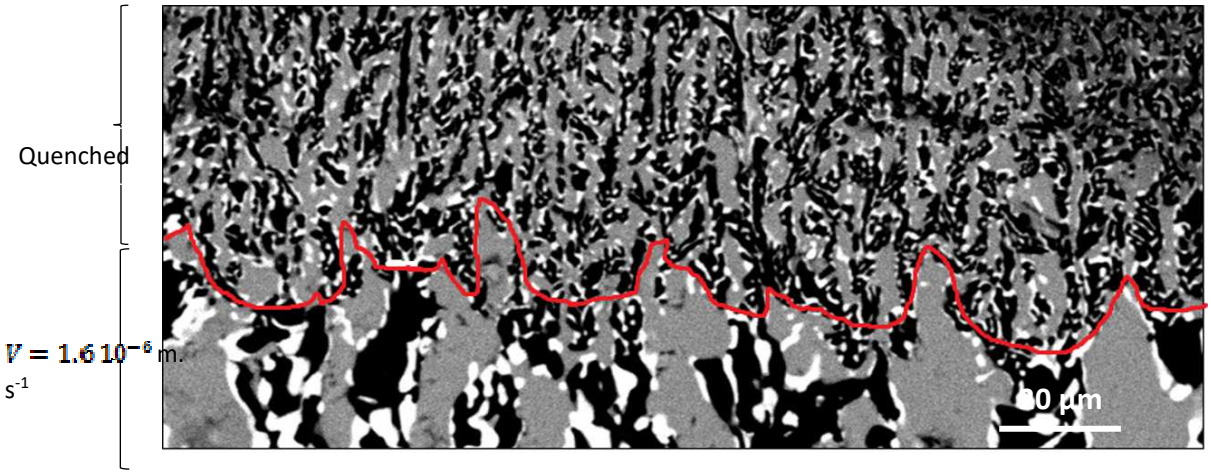

a)

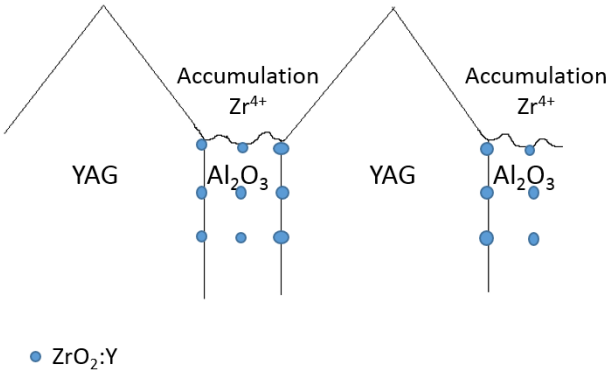

b)

Figure 9: a) Structure of a sample solidified at 1.6 10^{-6} m.s^{-1}, then quenched by increasing the pulling rate. The red line shows the quenched solid-liquid interface. b) Schematic of the solid-liquid interface. The zirconia phase, while appearing as precipitates, is in fact continuous.

The kinetic coefficients, μ, of YAG and alumina were measured, by aero-acoustic experiments, as respectively $3.5\ 10^{-5}$ m.s^{-1}.K^{-1} [44] and $5.\ 10^{-2}$ m.s^{-1}.K^{-1} [45]. Due to the complexity of the crystal structures, these values are much lower than for metals (order of unity). From the growth rate, which is equal for both phases, the kinetic undercooling, ΔT_k, can be computed:

$$\Delta T_k = \frac{V}{\mu} . \quad (6)$$

At $1.6\ 10^{-6}$ m.s^{-1}, this gives an undercooling of $4.7\ 10^{-2}$ K for YAG and $3.33\ 10^{-5}$ K for alumina. Considering a temperature gradient in the liquid $3.5\ 10^{3}$ K.m^{-1}, the YAG facets should protrude by 13 µm toward the liquid, this is in good agreement with the figure 9-a).

Song et al. [46] applied the irregular eutectic growth model proposed by Magnin and Kurz [47] to the growth of Al_2O_3-YAG. The agreement was good, taking into account the lack of precise data concerning the physical parameters used for the model. There is no theoretical model of the growth of facetted eutectics nor of ternary eutectics. So, we will use the classical facetted-rough binary eutectic, with two strong assumptions:

- The ZrO_2 is a minor phase, which does not impact significantly the alumina-YAG coupled growth.
- The facetted character of alumina can be neglected with respect to the YAG facets.

The model from Magnin et al. [47,48] on irregular eutectics allows computing the smallest spacing, corresponding to the smallest undercooling, and the largest spacing, above which lamellas split. The equations derived in this model are as follows:

$$< \lambda^2 > V = \phi^2 \frac{K_r}{K_c} \quad , \quad (7)$$

with $K_r = \frac{\bar{m} C_0}{D_l} \times \frac{P}{f_{YAG} f_{Al_2O_3}}$, $K_c = 2\bar{m} \left(\frac{\Gamma_{Al_2O_3} \sin\theta_{Al_2O_3}}{|m_{Al_2O_3}| f_{Al_2O_3}} + \frac{\Gamma_{YAG} \sin\theta_{YAG}}{|m_{YAG}| f_{YAG}} \right)$

and $\phi = \frac{<\lambda>}{\lambda_{ex}}$.

(8)

In these equations, C_0 is the length of the eutectic tie line, $\overline{m}$ is the half harmonic mean value of liquidus slopes, D_l is the diffusion coefficient, and Γ_l is the Gibbs-Thomson coefficient of phase *l*. The parameters $m_{Al_2O_3}$, m_{YAG}, f_{YAG} and $f_{Al_2O_3}$ are determined with the ThermoCalc software and the TCOX5 database along the eutectic valley. *P* is a Fourier series depending on lamellae extension. The liquidus slopes can be considered as constant. However the volume fraction of the phases changes with the ZrO_2 concentration (see table 3). The other physical parameters are given in table 4.

Table 3: Thermodynamic parameters as determined with ThermoCalc.

ZrO_2 (mol %)	$m_{Al_2O_3}$(K.mol%$^{-1}$)	m_{YAG}(K.mol%$^{-1}$)	f_{YAG}	$f_{Al_2O_3}$	$\frac{f_{Al_2O_3}}{f_{YAG}}$
0	-26,8	25,7	53,7	43,3	0,86
0,05	-24,6	21,9	52,6	43,03	0,81
0,1	-21,5	19,6	51	39	0,77
0,15	-27,7	19,9	50	36	0,71
0,179	-31,1	20	49,8	34	0,68

Table 4: Physical parameters used for the model.

Property	YAG	Al_2O_3	Reference
C_e (mol%)		20,3	ThermoCalc
C_0 (mol%)		37,5	ThermoCalc

D_l ($m^2.s^{-1}$)	5×10^{-9}	5×10^{-9}	[49]
Γ_i (K.m)	1×10^{-7}	$2{,}47 \times 10^{-7}$	[49]
θ_i	45	45	Estimated (Figure 9)

The model gives:

$$\langle\lambda\rangle^2 V = Cte = 6.10^{-17} m^3.s^{-1}, \quad (9)$$

very close to the experimental value, Equ. (3). A sensibility analysis was performed by changing the D_l and Γ_l values by ±90%: the calculated values of the *Cte* changed by less than one order of magnitude, the more sensible parameter being the diffusion coefficient (see [7] for more details). Introducing the effect of zirconia on the constitutional undercooling of the two other phases has no effect as it does not change the extremum conditions. Further, Magnin et al. [48] have shown that the kinetic undercooling has no effect on the lamellar spacing. The measured value of the ϕ parameter is 2, obtained from the mean spacing values shown on Table 2, and from the smallest spacing found by the intercept method. The theoretical value is 1.6, in reasonable agreement .This parameter is less sensitive to the choice of the physical constants.

7. Conclusion

The results obtained during this study on the Al_2O_3-YAG-ZrO_2:Y eutectic structure of EFG grown plates, give a better, while still incomplete, understanding of its solidification:

- The solid-liquid interface shows a strongly facetted YAG phase while the alumina has much smaller facets. Zirconia is rejected by the two other phases and grows at their junction or in depressions at the alumina-liquid interface.

- This is a truly coupled simultaneous growth of the three phases that are therefore continuously extending all along the growth direction. It should be noted that our

experiments performed with a laboratory X-Ray tomograph, concluded to a discontinuous ZrO_2 phase. Only synchrotron X-ray tomography was sensitive enough to demonstrate that it is indeed continuous.

- Restricting the analysis to a coupled growth of alumina and YAG only, shows a good fitting to the classical Magnin et al. model that was established and assessed for metallic binary systems. However, the alumina takes the place of the rough phase, while it is clear that it is indeed facetted, this shows that coupled growth is also possible for high melting entropy systems. Interphase surfaces were measured by Wang et al. [17] giving only 29% for the Al_2O_3/YAG surface. It is therefore surprising that zirconia, which occupies most of the surfaces but is neglected in the model, does not seem to impact significantly the eutectic spacing.

- The resulting structure is composed of two intricately entangled Al_2O_3 and YAG single crystals, with the zirconia phase conforming to the shape of a tridimensional net.

- The ternary solid-liquid interface can show colonies in case of growth parameters exceeding critical values. The reconstructed shape of the solidification interface shows rather low and flat cells. In the case of our samples, experimental studies suggest that the segregated species was Zr^{4+}, probably because an off-eutectic initial composition, in spite of careful preparation of the raw material.

There is still a number of uncertainties to solve in order to get a fully comprehensive understanding of this eutectic growth. An interesting question, with fundamental interest, concerns the role of the minor phase zirconia in the eutectic coupled growth. Precise measurement of physical properties would allow a more quantitative comparison to Magnin, or other, growth model. Also, it would be of interest to study the generalization of these conclusions to comparable eutectics, such as Al_2O_3-$Er_3Al_5O_{12}$-ZrO_2:Y or Al_2O_3-$MgAl_2O_4$-ZrO_2.

Acknowledgments

This research was funded by the ANR MatetPro CINATRA project, ref. ANR-12-RMNP-0008. We are indebted to the project coordinators from the SAFRAN Company, initially Amélie Potelle, then Michaël Podgorski. The present paper could not have existed without the confidence, help and friendship of the CINATRA partners at: RSA le Rubis (Nicolas Barthalay), ONERA (Michel Parlier, Marie-Hélène Ritti, Sylvie Lalanne, Jean-Claude Daux, Johan Petit, Roger Valle), ILM-Lyon (Omar Benamara, Kheirreddine Lebbou) and ICMPE-Thiais (Laura Londaitzbehere, Léo Mazerolles).

Nomenclature

C_e	Eutectic composition
C_i	Initial composition of the alloy
Cte	A constant
D_l	Diffusion coefficient in the liquid
G	Temperature gradient in the liquid
V	Growth rate
V_{local}	Local growth rate
V_{tip}	Growth rate at the tip of the cell
d_c	Colony diameter
f	Volume fraction
m_i	Liquidus slope of phase i
$\overline{m}$	Half harmonic mean value of liquidus slopes

$\bar{r}_i$	Mean size of phase *i*
θ_i^L	Angle of phase *i* at triple line
θ	Angle between two growth directions
λ	Eutectic spacing
λ_{ex}	Minimal value of eutectic spacing
μ	Linear kinetic coefficient
Γ	Gibbs Thomson coefficient
ΔT_k	Kinetic undercooling
ϕ	Ratio of mean to minimal eutectic spacing

Bibliography

[1] Y. Waku, H. Ohtsubo, N. Nakagawa, Y. Kohtoku, *Sapphire matrix composites reinforced with single crystal YAG phases*, J. Mat. Science **31** (1996) 4663-4670.

[2] J.I. Peña, M. Larsson, R.I. Merino, I. de Francisco, V.M. Orera, J. Llorca, J.Y. Pastor, A. Martin, J. Segurado, *Processing, microstructure and mechanical properties of directionally solidified Al_2O_3-$Y_3Al_5O_{12}$-ZrO_2 ternary eutectics*, J. Eur. Ceram. Soc. **26** (2006) 3113-3121.

[3] T. Nagira, H. Yasuda, S. Takeshima, T. Sakimura, Y. Waku, K. Uesugi, *Chain structure in the unidirectionally solidified Al_2O_3-YAG-ZrO_2 eutectic composite*, J. Cryst. Growth. **311** (2009) 3765-3770.

[4] Y. Waku, S-I. Sakata, A. Mitani, K. Shimitsu, *A novel oxide composite reinforced with a ductile phase for very high temperature structural materials*, Mat. Res. Innov. **5** (2001) 94-100.

[5] L. Carroz, T. Duffar, *Tuning the sapphire EFG process to the growth of Al_2O_3/YAG/ZrO_2:Y eutectic* J. Crystal Growth **489** (2018) 5-10.

[6] L. Carroz, « *Etude et mise en œuvre d'un procédé de préformage d'un alliage eutectique d'oxydes* » PhD Thesis, Univ. Grenoble-Alpes, 12 December 2016. *(In French)*

[7] M. Cherif « *Croissance de la céramique Al_2O_3-YAG-ZrO_2:Y et étude de la microstructure Chinese Script* » PhD Thesis, Univ. Grenoble-Alpes, 15 September 2016. *(In French)*

[8] C. Stelian, M. Cherif, L. Carroz, N. Barhalay, T. Duffar, *Growth rate effect on colony formation in directional solidification of Al_2O_3/YAG/ZrO_2,* J. American Ceramic Society **102** (2019) 2999-3008.

[9] O. Fabrichnaya, F. Aldinger, *Assessment of thermodynamic parameters in the system ZrO_2-Y_2O_3-Al_2O_3*, Z. Mettalkd. **95** (2004) 27-39.

[10] S.N. Lakiza, L.M. Lopato and A. V. Shevchenko, *Interactions in the Al_2O_3-ZrO_2-Y_2O_3*, Powder Met. and Metal Ceram. **33** (1994) 9-10.

[11] Y. Mizutami, H. Yasuda, I. Ohnaka, A. Sugiyama, S. Takeshima, M. Kirihara, Y. Waku, *Undercooled melt formation of metastable eutectic structure in Al_2O_3-Y_2O_3-ZrO_2 system*, Mat. Trans. **43** (2002) 2847-2854.

[12] A. Julian-Jankowiak, R. Valle, M. Parlier, *Potential of innovative ceramics for turbine applications,* Materials at High Temperatures **33** (2016) 578-585.

[13] O. Benamara, M. Cherif, T. Duffar, K. Lebbou, *Microstructure and crystallography of Al_2O_3-YAG-ZrO_2 ternary eutectic oxide grown by the micropulling down technique* J. Crystal Growth **429** (2015) 27-34.

[14] V. Boulos, L. Salvo, V. Fristot, P. Lhuissier, D. Houzet, *Investigating performance variations of an optimized GPU-ported granulometry algorithm*, 18th International European Conference on Parallel and Distributed Computing, Rhodes Island, Greece (2012).

[15] Y. Murayama, S. Hanada, J.H. Lee, A. Yoshikawa, and T. Fukuda, *Microstructure and high temperature strength of directionally solidified $Al_2O_3/Y_3Al_5O_{12}/ZrO_2$ eutectic composite*, Mater. Trans. **45** (2004) 303-306.

[16] O. Benamara, K. Lebbou *Shaped ceramic eutectic plates grown from the melt and their properties* J. Crystal Growth **449** (2016) 67-74.

[17] X. Wang, Y. Zhong, D. Wang, L. Sun, B. Jiang, J. Wang *Effect of interfacial energy on microstructure of a directionally solidified Al_2O_3/YAG eutectic ceramic,* J. Am. Ceram. Soc. **101** (2018) 1029-1035.

[18] R.I. Merino, Communication during the Vth Directionally Solidified Eutectic Ceramics Workshop, Warsaw, April 3–7, 2016.

[19] E. Boller, P. Tafforeau, W. Ludwig, L. Helfen, T. Weitkamp, et al., *Techniques d'imagerie pour la caracterisation 3D des matériaux à l'ESRF*. Conf. Matériaux 2010, October 2010, Nantes, France.

[20] http://simap.grenoble-inp.fr/en/research/x-ray-tomographies-of-directionally-solidified-ternary-oxide-alloys.

[21] H. Su, J. Zhang, L. Liu and H. Fu*, Preparation and microstructure evolution of directionally solidified $Al_2O_3/Y_3Al_5O_{12}$/YSZ ternary eutectic ceramics by a modified electron beam floating zone melting*, Mat. Lett. **91** (2013) 92-95.

[22] J.H. Lee, A. Yoshikawa, T. Fukuda, Y. Waku, *Growth and characterization of $Al_2O_3/Y_3Al_5O_{12}/ZrO_2$ ternary eutectic fibers,* J. Cryst. Growth **231** (2001) 115-120.

[23] H.E. Exner, H.P. Hougardy, *Quantitative image analysis of microstructures*. DGM Informations- gesellschaft Verlag, Oberursel, (1988), 235 pp.

[24] Y. Mizutami, H. Yasuda, I. Ohnaka, N. Maeda, Y. Waku, *Coupled growth of unidirectionally solidified Al_2O_3–YAG eutectic ceramics*, J. Cryst. Growth **244** (2002) 384-392.

[25] L.E. Matson, N. Hecht, *Microstructural stability and mechanical properties of directionally solidified Alumina/YAG eutectic monofilaments*, J. Eur. Ceram. Soc **19** (1999) 2487-2501.

[26] A. Sayir, *in "Computer-aided design of high temperature materials"* Oxford university press, Inc. (1999) 197-211.

[27] A. Yoshikawa, B.M. Epelbaum, K. Hasegawa, S.D. Durbin, *Microstructure in oxide eutectic fibers grown by a modified micro-pulling-down method*, J. Cryst. Growth **205** (1999) 305-316.

[28] A. Yoshikawa, K. Hasegawa, J.H. Lee, S.D. Durbin, B.M. Epelbaum, D.H. Yoon, T. Fukuda, Y. Waku, *Phase identification of Al_2O_3/$REAlO_3$ (RE=Sm-Lu, Y)* eutectics, J. Cryst. Growth **218** (2000) 67-73.

[29] J.I. Peña, R.I. Merino, N.R. Harlan, A. Larrea, G.F. de la Fuente, V.M. Orera, *Microstructure of Y_2O_3 doped Al_2O_3-ZrO_2 eutectics grown by the laser floating zone method*, J. Eur. Ceram. Soc. **22** (2002) 2595-2602.

[30] T. Mah, T.A. Parthasarathy, M.D. Petry and L.E. Matson, *Processing, microstructure and properties of Al_2O_3-$Y_3Al_5O_{12}$(YAG) eutectic fibers*, Proceedings of the 17th annual conference on Composites and Advanced ceramic materials, Part 1 of 2: Ceram. Eng. Science Proceedings, **14** (2008) 622-638.

[31] H. Su, J. Zhang, C. Cui, L. Liu and H. Fu, *Rapid solidification of Al_2O_3/$Y_3Al_5O_{12}$(YAG) binary eutectic ceramic in situ composites*, Mat. Science Eng. A **479** (2008) 380-388.

[32] D. Viechnicki, F. Schmid, *Eutectic Solidification in the System Al_2O_3 /$Y_3Al_5O_{12}$*, J. Mat. Sci. **4** (1969) 84-88.

[33] S.N. Lakiza, *Directional solidification of eutectics: new prospects for refractory oxide ceramics (review)*, Translated from Poroshkovaya Metallurgiya **320** (1989) 58-69.

[34] H. Su, J. Zhang, L. Liu and H. Fu, *Processing, microstructure, and properties of laser remelted $Al_2O_3/Y_3Al_5O_{12}$(YAG) eutectic in situ composite*, Trans. Nonferrous Met. Soc. China **17** (2007) 1259-1264.

[35] R. Cicka, V. Trnovcova, M. Yu, Starostin, O. Bosak, *Microstructure and electrical properties of near-eutectic alumina-zirconia composites*, J. Optoelectronics Adv. Mat. **8** (2006) 1460-1465.

[36] J. Echigoya, Y. Takabayashi, H. Suto, M. Ishigame, *Structure and crystallography of directionally solidified Al_2O_3-ZrO_2-Y_2O_3 eutectic by the floating zone melting method*, J. Mat. Science Letters **5** (1986) 150-152.

[37] V.N. Savushkin, M. D. Lyubalin and V.A. Pis'mennyi, *Physical properties of composite material obtained by controlling crystallization of fusions in the Al_2O_3-$ZrO_2(Y_2O_3)$ system*, Refractories **34** (1993) 584-586.

[38] V. Trnovcová, M. Starostin, V. Labas and R. Cicka, *Microstructure and Physical properties of directionally solidified alumina-zirconia eutectic composites*, Ionics **4** (1998) 275-284.

[39] F.J. Ester, A. Larrea, R.I. Merino, *Processing and microstructural study of laser remelted Al_2O_3-YSZ-YAG eutectic plates*, J. Eur. Ceram. Soc. **31** (2011) 1257-1268.

[40] X-S. Fu, G-Q Chen, Y-F. Zu, J-T. Luo, W-L. Zhou, *Microstructures refinement of melt-grown Al_2O_3/YAG/ZrO_2 eutectic bulk*, Ceram. Int. **39** (2013) 7445-7452.

[41] K. Song, J. Zhang, X. Jia, H. Su, L. Liu, H. Fu, *Longitudinal cross-section microstructure of growth striation in $Al_2O_3/Y_3Al_5O_{12}/ZrO_2$ directionally solidified eutectic ceramic prepared by laser floating zone*, J. Eur. Ceram. Soc. **33** (2013) 1123-1128.

[42] H.W. Weart and D.J. Mack, *Eutectic solidification structures*, Trans. Metall. Soc. AIME **212** (1958) 664-671.

[43] M. Cherif, P. Hicher, O. Benamara, K. Lebbou, R. Haumont, T. Duffar, *Electric Field Effects During Solidification of the Ternary Oxide Eutectic Al_2O_3-YAG-ZrO_2* Crystal Research and Technology **53** (2018) 1700251.

[44] K. Nagashio and K. Kuribayashi, *Rapid solidification of $Y_3Al_5O_{12}$ garnet from hypercooled melt*, Acta mater. **49** (2001) 1947-1955.

[45] M. Li and K. Kuribayashi, *Growth kinetics of highly undercooled Al_2O_3 melts*, J. Appl. Phys. **95** (2004) 2342-2347.

[46] K. Song, J. Zhang, X. Jia, H. Su, L . Liu, H. Fu, *Solidification microstructure of laser floating zone remelted Al_2O_3-YAG eutectic in situ composite*, J. Cryst. Growth **345** (2012) 51-55.

[47] P. Magnin and W. Kurz, *An analytical model of irregular eutectic growth and its application to Fe-C,* Acta metall. **35** (1987) 1119-1128.

[48] P. Magnin, J.T. Mason and R. Trivedi, *Growth of irregular eutectics and the Al-Si system*, Acta Metal. Mater. **39** (1991) 469-480.

[49] K. Song, J. Zhang, X. Lin, L. Liu, W. Huang, *Microstructure and mechanical properties of $Al_2O_3/Y_3Al_5O_{12}/ZrO_2$ hypereutectic directionally solidified ceramic prepared by laser floating zone*, J. Eur. Ceram. Soc. **34** (2014) 3051-3059.